Supporting Information

Catalytic Consequences of Oxidant, Alkene, and Pore Structure on Alkene Epoxidations within Titanium Silicates

Daniel T. Bregante, Jun Zhi Tan, Rebecca L. Schultz, E. Zeynep Ayla,

David S. Potts, Chris Torres, and David W. Flaherty*

Department of Chemical and Biomolecular Engineering

University of Illinois at Urbana-Champaign, Urbana, IL 61801, USA

*Corresponding Author

Phone: +1 217-244-2816

Email: dwflhrty@illinois.edu

S1.0 Catalyst Characterization

S1.1 X-Ray Diffraction

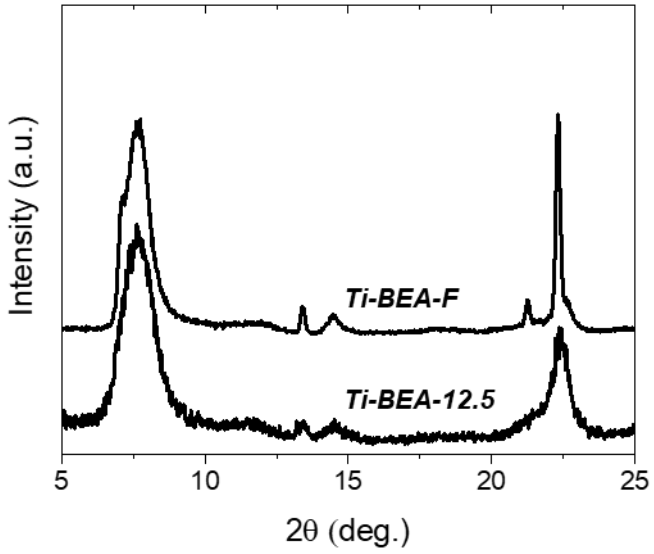

Figure S1. X-ray diffractograms for Ti-BEA-12.5 and Ti-BEA-F. Diffractograms are vertically offset for clarity.

Figure S1 shows X-ray diffractograms for Ti-BEA-12.5 and Ti-BEA-F contain distinct crystallographic features that are a hallmark of the *BEA framework. It should be noted that the sharpness in the 22.4 degree feature in Ti-BEA-F indicates a high degree of crystallinity. Ti-BEA-12.5 contains broad diffraction features that are indicative of internal defects that form upon dealumination and synthesis in hydroxide media.

S1.2 Diffuse Reflectance UV-vis Spectra

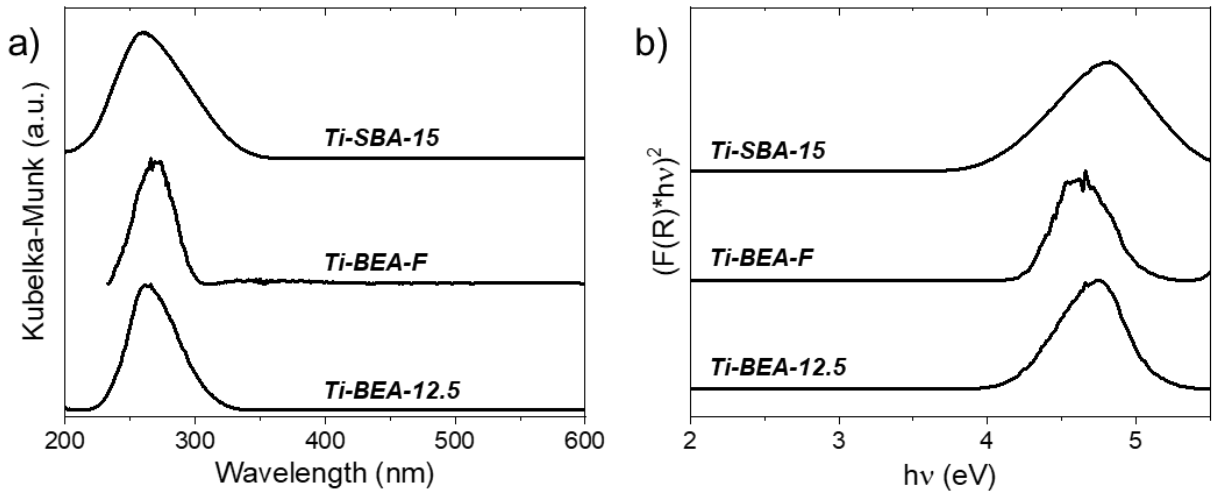

Figure S2. a) Diffuse reflectance UV-vis spectra and b) Tauc plots for Ti-BEA-12.5, Ti-BEA-F, and Ti-SBA-15. All plots were normalized to the most intense feature and are vertically offset for clarity. Spectra were collected at ambient conditions.

Figure S2 shows that Ti-BEA-12.5, Ti-BEA-F, and Ti-SBA-15 contain a single UV-vis absorbance feature around 260 nm or 4.7 eV. The leading edge was fit using a line to extrapolate the x intercept, which is equal to the band gap of the material. In all cases, the UV-vis absorbance features is qualitatively consistent with hydrated, isolated Ti^{4+} sites.[1] Ti atoms do not likely exist as oligomers or metal oxide nanoparticles, because these structures would occlude significant fractions of the Ti atoms and lead to lower percentages of Ti atoms that form active sites and catalyze alkene epoxidation."

S1.3 Energy Dispersive X-Ray Fluorescence

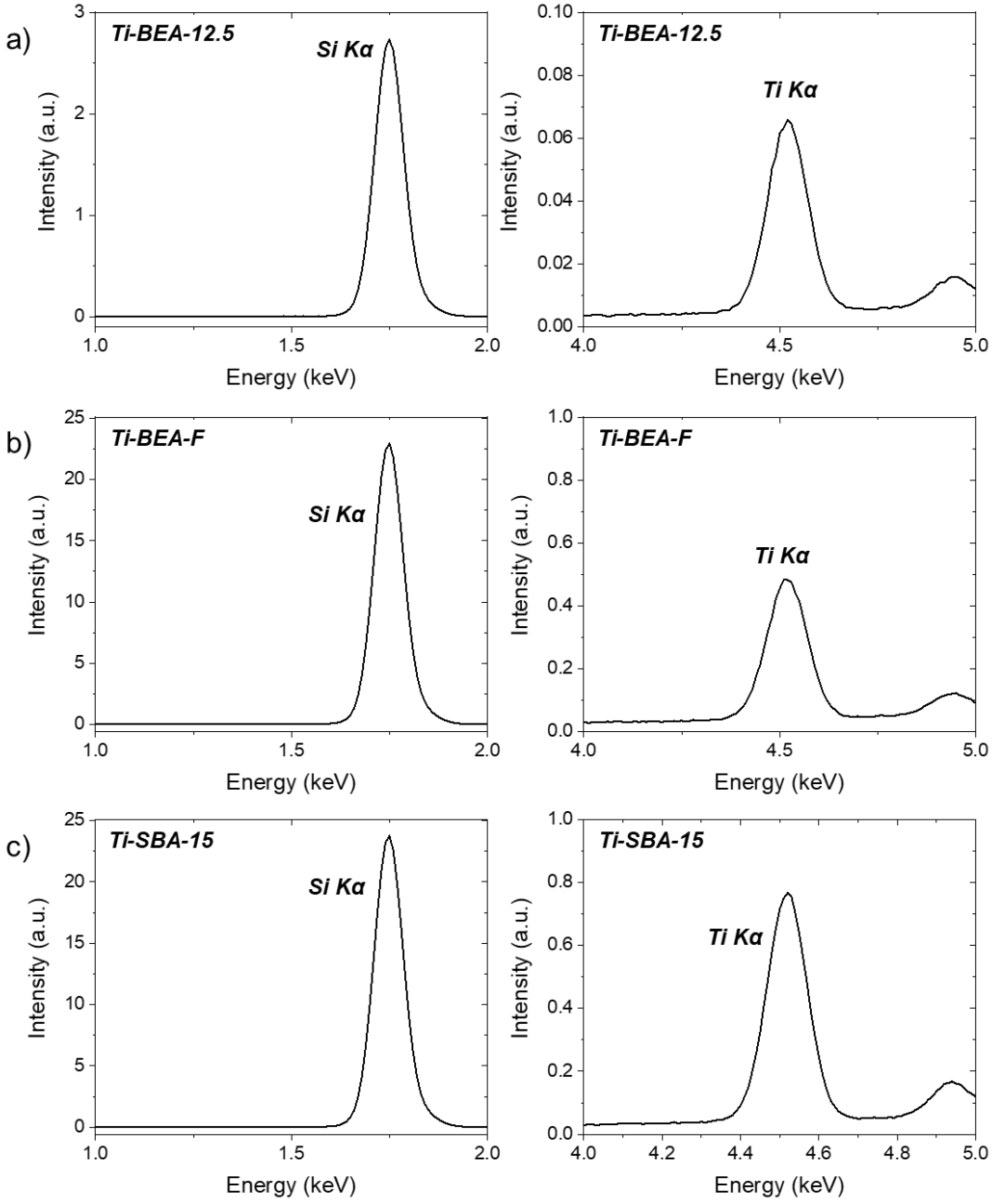

Figure S3. Energy dispersive X-ray fluorescence (EDXRF) spectra of a) Ti-BEA-12.5, b) Ti-BEA-F, and c) Ti-SBA-15 materials. The plots have been separated into two panels (left and right) for each material to facilitate comparisons among spectra.

S1.4 N_2 Physisorption on Ti-Silicates

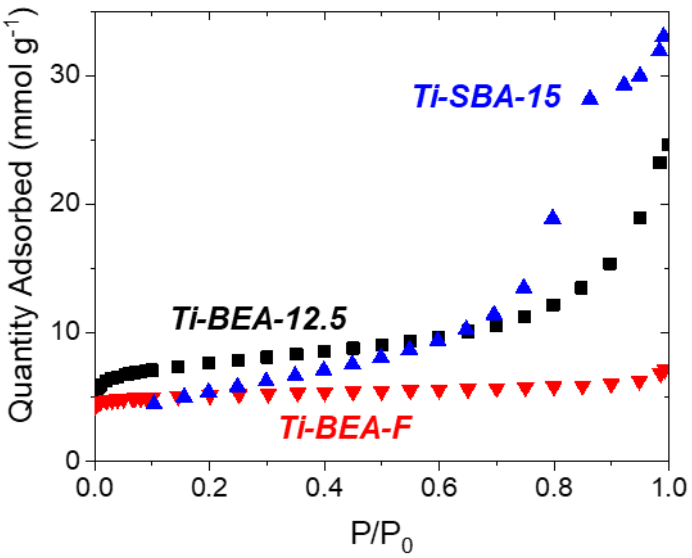

Figure S4. Nitrogen adsorption isotherms (77 K) over Ti-BEA-12.5 (■), Ti-BEA-F (▼), and Ti-SBA-15 (▲).

S1.5 Uptake of C_8H_{16} into Si-BEA-12.5 and SBA-15

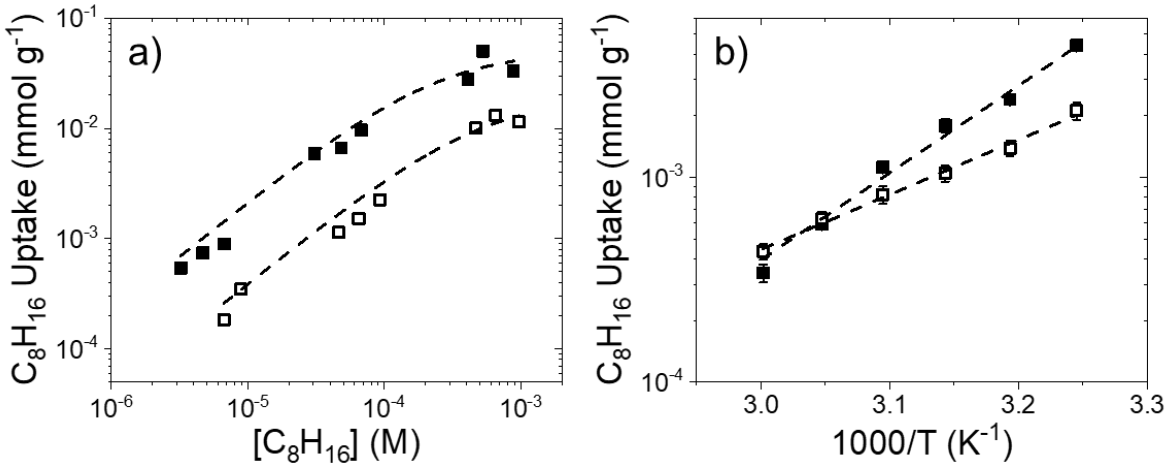

Figure S5. 1-Octene uptake (*per gram of solid*) into Si-BEA-12.5 (solid symbols) or SBA-15 (open symbols) as a (a) function of C_8H_{16} concentration at 313 K and (b) inverse temperature (0.05 mM C_8H_{16}) in CH_3CN. The dashed curves in panel (a) represent least regression fits of a Langmuir isotherm, while those in panel (b) are linear fits whose slopes are proportional to the enthalpy of C_8H_{16} adsorption (ΔH_{Ads}).

Figure S5 shows that C_8H_{16} uptake into Si-BEA-12.5 and SBA-15 is Langmuirian, where uptake is proportional to $[C_8H_{16}]$ at low concentrations of C_8H_{16} (<0.1 mM) and approaches saturation at high $[C_8H_{16}]$. Adsorption enthalpies for C_8H_{16} into these two porous materials was determined through van't Hoff analysis of C_8H_{16} uptake under conditions where C_8H_{16} uptake is proportional to $[C_8H_{16}]$.

S1.6 *Tert*-butyl Phosphonic Acid Active Site Titrations

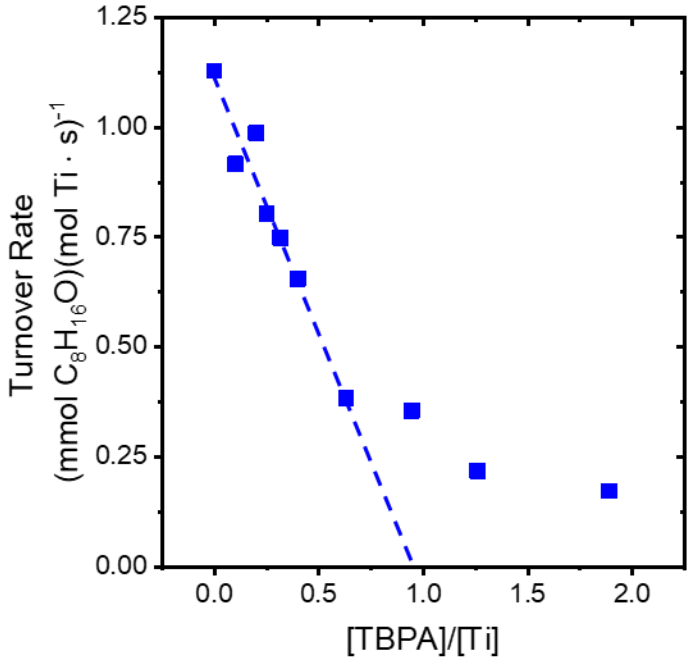

Figure S6. Turnover rates for $C_8H_{16}O$ formation as a function of *tert*butyl phosphonic acid to Ti ratio ([TBPA]/[Ti]; 0.01 M H_2O_2, 0.01 M C_8H_{16}) over Ti-SBA-15. The dashed line represents a linear regression to the first 7 points, with the y-intercept set to the turnover rate in the absence of the TBPA titrant.

Figure S6 shows how the turnover rate for C_8H_{16} epoxidation varies with the ratio of *tert*buyl phosphonic acid (TBPA) titrant to Ti atoms within Ti-SBA-15. At low ratios of [TBPA]/[Ti], turnover rates decrease linearly with [TBPA]/[Ti], which suggests that these active sites are catalytically equivalent. As the rato of [TBPA]/[Ti] increases further, the rates continue to decrease in a non-linear fashion, which may result from the equilibria of TBPA molecules binding to Ti active sites. The linear portion of this plot is extended to the x-axis intercept, where the ratio of [TBPA]/[Ti] ratio that yields an expected turnover rate of zero (95 ± 4 %) represents the percent of active Ti atoms within Ti-SBA-15.

S2.0 Time Resolved *In Situ* UV-Vis

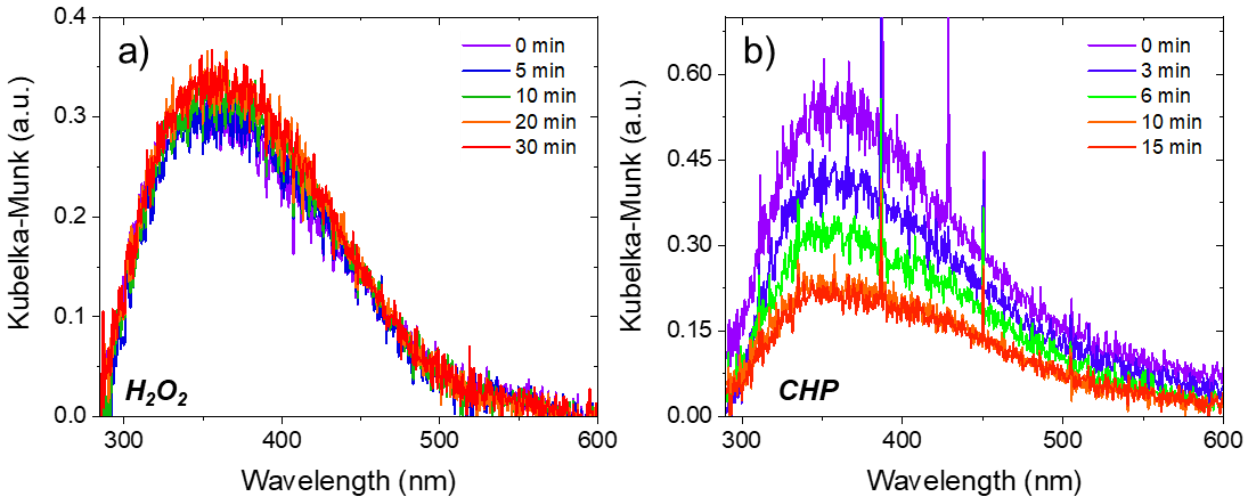

Figure S7. UV-vis spectra of Ti-BEA-12.5 at the indicated times (see legend) as CH_3CN (39 mM H_2O, 313 K) flowed over a) H_2O_2 (10 mM H_2O_2, 39 mM H_2O) or b) CHP-activated (0.3 M CHP, 39 mM H_2O) Ti-BEA-12.5.

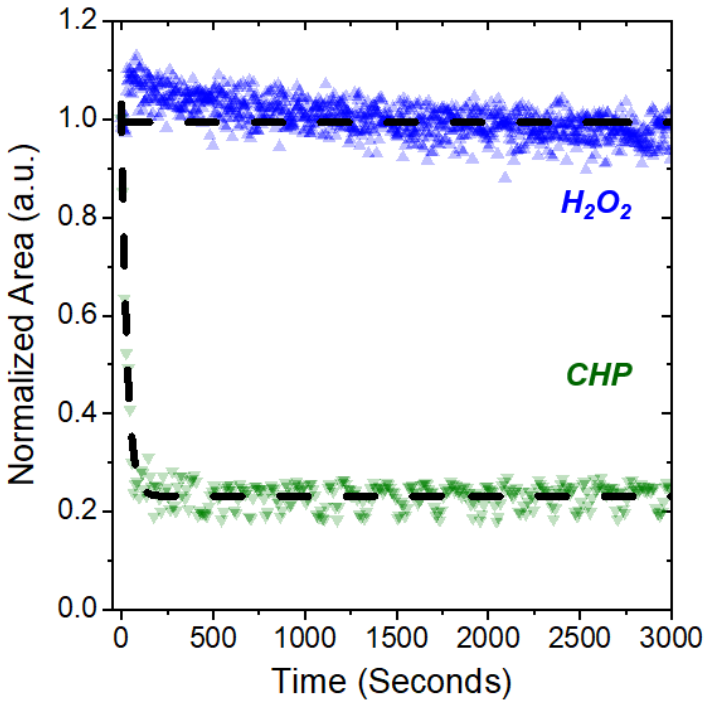

Figure S8. Areas for the LMCT bands of Ti-OOH + Ti-(η^2-O_2) (▲) and Ti-OOcumyl (▼) as a function of time as CH_3CN (39 mM H_2O, 313 K) flowed over H_2O_2- or CHP-activated Ti-SBA-15, respectively. The dashed black curve for H_2O_2 is meant to guide the eye, while the curve for CHP represents an exponential decay fit with a decay constant (k_d) of $3.3 \cdot 10^{-2}$ s^{-1}. All areas were normalized to the initial area (i.e., at time = 0) before introduction of the oxidant-free CH_3CN solution.

S3.0 1-Octene Epoxidation Kinetics

S3.1 Effect of H_2O Concentration of 1-Octene Epoxidation Rates

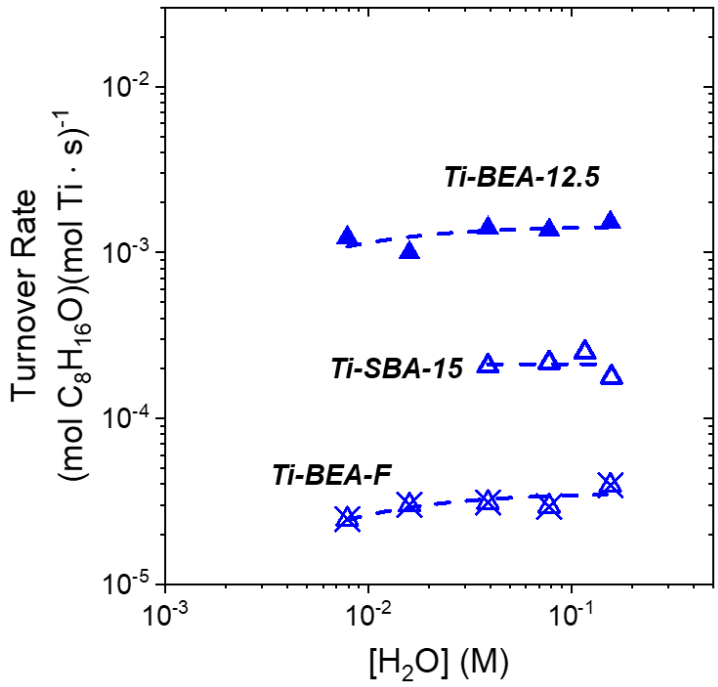

Figure S9. Turnover rates for $C_8H_{16}O$ formation as a function of [H_2O] in Ti-BEA-12.5 (▲; 0.3 mM $C_8H_{16}O$, 10 mM H_2O_2), Ti-BEA-F (△ with an "X"; 0.3 mM $C_8H_{16}O$, 10 mM H_2O_2), and Ti-SBA-15 (△; 10 mM C_8H_{16}, 10 mM H_2O_2) in CH_3CN at 313 K. Dashed lines represent fits to equation 2a. Rates of epoxidation over Ti-BEA-12.5 and Ti-BEA-F were reported initially in ref [2].

S3.2 Comparisons of Rates of C_8H_{16} Epoxidation and H_2O_2 Decomposition

Reaction conditions that result in turnover rates for C_8H_{16} epoxidation that are proportional to $[C_8H_{16}]$ and are independent of $[H_2O_2]$ (Section 3.2) are described by the following rate expression

$$\frac{r_E}{[L]} = k_4[C_8H_{16}] \quad \text{(S1)}$$

Equation S1 shows that extrapolation of the linear portion of Figures 3a and 3b allow us to estimate the value of $k_4[C_8H_{16}]$ under conditions where $C_8H_{16}O$ saturates Ti active sites. Similarly, the rates of H_2O_2 decomposition ($2.7 \cdot 10^{-3}$ (mol H_2O_2)(mol Ti $\cdot$ s)$^{-1}$) are equal to values of $k_6[H_2O_2]$.

Table S1. Calculated ratios of $k_4[C_8H_{16}]$:$k_6[H_2O_2]$ for Ti-BEA-12.5 (50 mM C_8H_{16}) and Ti-SBA-15 (1 M C_8H_{16}) using interpolated values from Figures 3a and 3b and H_2O_2 decomposition rates.

Sample	$k_4[C_8H_{16}]$:$k_6[H_2O_2]$
Ti-BEA-12.5	11
Ti-SBA-15	8

Table S1 shows that under conditions where C_8H_{16} epoxidation rates are invariant with $[C_8H_{16}]$ (i.e., ~50 mM on Ti-BEA-12.5 and 1 M on Ti-SBA-15) the ratio of $k_4[C_8H_{16}]$:$k_6[H_2O_2]$ are >>1, which allows for the simplification of equation 2a within the main text (Section 3.2).

S4.0 Changes in Epoxidation Rate with 1-Alkene Chain Length

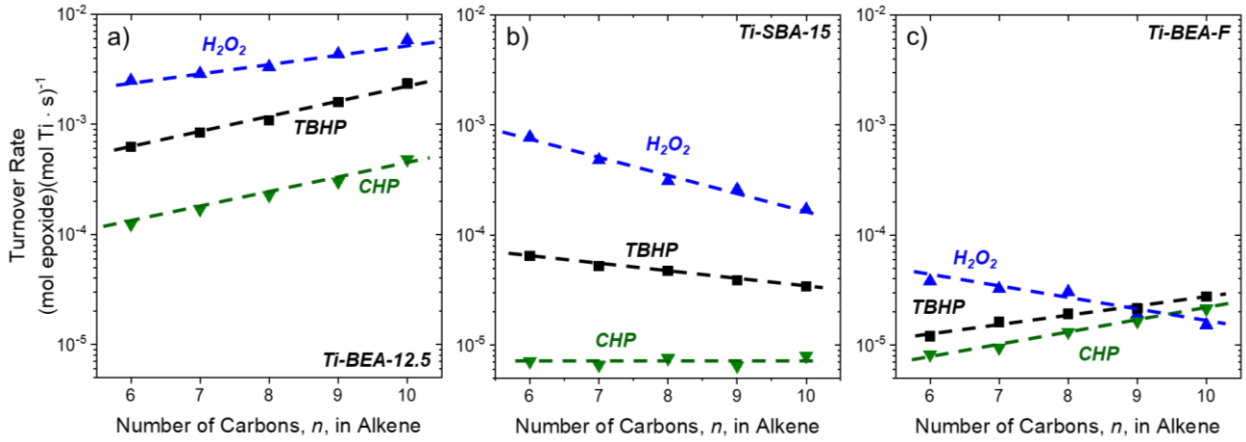

Figure S10. Turnover rates for C_nH_{2n} (n = 6 – 10; for 1-alkenes) epoxidation as a function of carbon number, n, over (a) Ti-BEA-12.5, (b) Ti-SBA-15) and (c) Ti-BEA-F with 10 mM H_2O_2 (▲), 10 mM TBHP (■), or 0.3 M CHP (▼) in CH_3CN (with 39 mM H_2O) at 313 K. Reactions with H_2O_2, TBHP, and CHP in panels (a) and (c) contained 0.5 mM, 10 mM, or 10 mM alkene, respectively. All reactions in panel (b) contained 10 mM alkene. Dashed lines are intended to guide the eye.

S5.0 Estimation of Solid Angles

The solid angle (Ω) provides a quantitative measure for the steric size of a ligand.[3] Specifically, values of Ω describe the surface area that a solid (e.g., a ligand) projects onto the surface of a sphere and is given by

$$\Omega = \int_S \frac{\boldsymbol{r} \cdot d\boldsymbol{S}}{\boldsymbol{r}^3} \tag{S2}$$

where $\boldsymbol{r}$ is the position vector of the element of the surface ($\boldsymbol{s}$; e.g., the sphere surrounding the complex) with respect to the vertex (e.g., the binding site). In this formalism, values of Ω take into account the shape of the ligands.

Scheme S1. A visual representation of a 1-octene epoxidation transition state with CHP. For clarity, the cumyl group (red) and aliphatic tail of 1-octene (blue) are color coded to visualize the two functions that are interacting through inner-sphere interactions. The strength of these interactions is presumed to be dependent on the steric bulk of these functional groups.

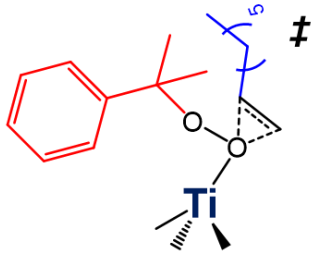

In the context of this manuscript, the two ligands investigated are the "-R" group connected to Ti-OOR intermediates and the aliphatic tail of the alkene (Scheme S1). Here, there are assumed to be two vertices, one at the distal oxygen atom that connects to the -R group of the Ti-OOR intermediate, and the 2-position of the 1-alkene. As such, the solid angles that describe the extent of the inner-sphere interactions between these species are those of the -R group or the tail of the alkene (e.g., a 1-butyl tail for 1-hexene).

Values of Ω have been tabulated for a variety of ligands and are widely available in a book chapter by White and Coville.[3] Table S2 shows values of Ω used within this study. Values of Ω that were not available were estimated through group-additivity methods.

Table S2. Solid angles (in steradians, Sr) for the indicated ligands.

Ligand	Ω (Sr)
-H	0
$-C(CH_3)_3$	3.32
$-C(CH_3)_2Ph$	3.71
$-CH_3$	0.80
$-CH_2CH_3$	1.64
$-(CH_2)_3CH_3$	2.45
$-(CH_2)_4CH_3$	2.85
$-(CH_2)_5CH_3$	3.26
$-(CH_2)_6CH_3$	3.66
$-(CH_2)_7CH_3$	4.07

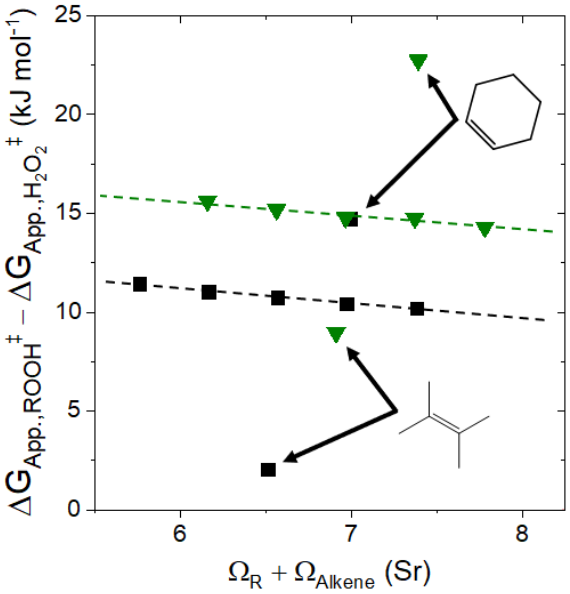

Figure S11. Differences in the apparent free energies of activation for alkene epoxidation with TBHP (■) or CHP (▼) relative to 1-alkene epoxidation with H_2O_2 over Ti-BEA-12.5 as a function of the solid angle of the alkene tail. Values of $\Delta G_{App}^{\ddagger}$ were calculated from turnover rates using equation 6. Dashed lines represent fits of equation 12 to the series of 1-alkenes.

Figure S11 shows how $\left(\Delta G_{App,ROOH}^{\ddagger} - \Delta G_{App,H_2O_2}^{\ddagger}\right)$ varies with $(\Omega_R + \Omega_{Alkene})$ for 1-alkene, cyclohexene, and 2,3-dimethyl-2-butene epoxidation. The values of Ω_R for cyclohexene and 2,3-dimethyl-2-butene were approximated by the sum of two -CH_2CH_3 or four -CH_3 groups, respectively. Values of $\left(\Delta G_{App,ROOH}^{\ddagger} - \Delta G_{App,H_2O_2}^{\ddagger}\right)$ for cyclohexene and 2,3-dimethyl-2-butene clearly deviate from the trend observed for 1-alkene epoxidation, which is likely attributed with the different electronic properties of these epoxidation transition states, relative to those for 1-alkene epoxidation. Specifically, the term $\left(G_{ROOH}^{\ddagger,0} - G_{H_2O_2}^{\ddagger,0}\right)$ is assumed to be constant as the alkene reactant is varied to determine the sensitivity of the reaction on the inner-sphere interactions among Ti-OOR intermediates with the substitution of the alkene reactant. When there is a change in the electronic properties of the C=C associated with changing the substituents, then values of $\left(G_{ROOH}^{\ddagger,0} - G_{H_2O_2}^{\ddagger,0}\right)$ are likely *not constant*, which necessitates an additional term (See section 3.5 in the main text) that corrects for how the *intrinsic* free energies of the transition states depends on the changes in alkene reactant.

S6.0 Limitations on Quantifying Inner-Sphere Interactions with Steric Factors

The application of equation 11 to determining how the kinetics of 1-alkene epoxidation depended on the size of the epoxidation transition states (i.e., $\Omega_R + \Omega_{Alkene}$) required that the electronic properties of the transition states not portray a measurable dependence on the length of the alkene (i.e., $\Delta G^{\ddagger}_{Int.,ROOH} - \Delta G^{\ddagger}_{Int.,H_2O_2}$) are equivalent for all 1-alkenes within this study. This assumption holds for 1-alkene epoxidation because the electronic properties of the C=C do not change significantly with the addition of a single methylene unit far from the double bond. Instead, if the structure of the alkene (or general reactant for other chemistries) is changed, such that the electronic properties of the C=C is also affected then this assumption will break down. When the electronic properties of the transition states vary concomitantly with the steric bulk of the reactive species, an additional factor (ψ) to equation 11 (or an analogously derived expression) may be added that accounts for the differences in the electronic properties.

$$\Delta G^{\ddagger}_{App,ROOH} - \Delta G^{\ddagger}_{App,H_2O_2} = \Delta G^{\ddagger}_{Int.,ROOH} - \Delta G^{\ddagger}_{Int.,H_2O_2} + \psi + \rho_{\ddagger,R}(\Omega_R + \Omega_{Alkene}) \quad \text{(S3)}$$

Here, ψ represents the difference in electronic properties of the transition states among two series of reactants (e.g., cyclic alkenes and 1-alkenes).

The theory developed here requires a measure of steric bulk. In this example, we used solid angles to quantify the interfacial area for interactions among Ti-OOR intermediates and the aliphatic tail of the 1-alkene. Here, we used group contribution methods to estimate values of Ω (Section S5), which may not be available for all types of functional groups. In cases where values of Ω are not available, this may be substituted for another measure of molecular size. For example, geometry optimization within molecular simulations can yield a quantitative measure of steric bulk which may be substituted in place of Ω to yield an analogous expression to equation 11.

References

1. Harris, J. W.; Arvay, J.; Mitchell, G.; Delgass, W. N.; Ribeiro, F. H., Propylene oxide inhibits propylene epoxidation over Au/TS-1. *J. Catal.* **2018,** *365*, 105-114.
2. Bregante, D. T.; Johnson, A. M.; Patel, A. Y.; Ayla, E. Z.; Cordon, M. J.; Bukowski, B. C.; Greeley, J.; Gounder, R.; Flaherty, D. W., Cooperative Effects between Hydrophilic Pores and Solvents: Catalytic Consequences of Hydrogen Bonding on Alkene Epoxidation in Zeolites. *J. Am. Chem. Soc.* **2019,** *141*, 7302-7319.
3. White, D.; Coville, N. J., Quantification of Steric Effects in Organometallic Chemistry. *Adv. Organomet. Chem.* **1994,** *36*, 95-158.